Carbohydrate Polymers 110 (2014) 195–202

Contents lists available at ScienceDirect

Carbohydrate Polymers

journal homepage: www.elsevier.com/locate/carbpol

Green synthesis of chondroitin sulfate-capped silver nanoparticles: Characterization and surface modification

Kuang-ming Cheng [a], Yao-wen Hung [a], Cheng-cheung Chen [a,b], Cheng-che Liu [a], Jenn-jong Young [a,*]

[a] Institute of Preventive Medicine, National Defense Medical Center, PO Box 90048-700, Sanhsia, New Taipei City 237, Taiwan, ROC
[b] Department of Food Science, National Taiwan Ocean University, 2 Pei-Ning Road, Keelung 20224, Taiwan, ROC

ARTICLE INFO

Article history:
Received 20 January 2014
Received in revised form 3 March 2014
Accepted 20 March 2014
Available online 28 March 2014

Keywords:
Green synthesis
Silver nanoparticles
Chondroitin sulfate
Chemical reduction
Dynamic light scattering
N-[(2-hydroxy-3-trimethylammonium)propyl]chitosan chloride

ABSTRACT

A one-step route for the green synthesis of highly stable and nanosized silver metal particles with narrow distribution is reported. In this environmentally friendly synthetic method, silver nitrate was used as silver precursor and biocompatible chondroitin sulfate (ChS) was used as both reducing agent and stabilizing agent. The reaction was carried out in a stirring aqueous medium at the room temperature without any assisted by microwave, autoclave, laser irradiation, γ-ray irradiation or UV irradiation. The transparent colorless solution was converted to the characteristics light red then deep red-brown color as the reaction proceeds, indicating the formation of silver nanoparticles (Ag NPs). The Ag NPs were characterized by UV–visible spectroscopy (UV–vis), photon correlation spectroscopy, laser Doppler anemometry, transmission electron microscopy (TEM), and Fourier-transform infrared spectroscopy (FT-IR). The results demonstrated that the obtained metallic nanoparticles were Ag NPs capped with ChS. In this report, dynamic light scattering (DLS) was used as a routinely analytical tool for measuring size and distribution in a liquid environment. The effects of the reaction time, reaction temperature, concentration and the weight ratio of ChS/Ag^+ on the particle size and zeta potential were investigated. The TEM image clearly shows the morphology of the well-dispersed ChS-capped Ag NPs are spherical in shape, and the average size (<20 nm) is much smaller than the *Z*-average value (76.7 nm) measured by DLS. Meanwhile, the ChS-capped Ag NPs coated with N-[(2-hydroxy-3-trimethylammonium) propyl] chitosan chloride (HTCC) were prepared by an ionic gelation method and the surface charge of Ag NPs was switched from negative to positive.

1. Introduction

Silver is a nontoxic, safe inorganic antibacterial agent used for centuries and is capable of killing more than 650 types of diseases causing microorganisms. It has a significant potential for a wide range of biological applications such as preventing infections, healing wounds, anti-inflammatory and use as an antibacterial agent for antibiotic resistant bacteria. Silver ions and its compounds are highly toxic to microorganisms exhibiting strong biocidal effects on many species of bacteria but only have a low toxicity toward animal cells. Therefore, silver ions are employed in formulation of dental resin composites, bone cement and coatings for medical devices, etc.

Recently, nanomedicine has become a leading research field. Scientists are involved in developing safe, effective, cheaper, and less toxic drugs or carriers to combat diseases like cancer, epilepsy, etc. These nanosized carriers have a site specific action thus only a safe dosage of drug molecules need to be administered and helps in reducing the undesired toxicity. Their small size gives them an advantage while evading the immune responses and also gives them the ability to cross relatively impermeable membranes (Amidi, Mastrobattista, Jiskoot, & Hennink, 2010).

One key aspect of nanotechnology concerns the development of rapid and reliable experimental protocols for the synthesis of nanomaterials over a range of chemical compositions, sizes, high monodispersity and large-scale production. A variety of techniques have been developed to synthesize silver metal nanoparticles, including chemical reduction, microemulsion (Zhang, Qiao, & Chen, 2006), γ-ray irradiation (Chen, Song, & Liu, 2007), laser ablation (Abid, Wark, Brevetm, & Girault, 2002), electrochemical method (Reicha, Sarhan, Abdel-Hamid, & El-Sherbiny, 2012;

* Corresponding author. Tel.: +886 2 81777038x19917; fax: +886 2 26736954.
E-mail addresses: jjyoung@ms49.hinet.net, 1959jjyoung@gmail.com (J.-j. Young).

http://dx.doi.org/10.1016/j.carbpol.2014.03.053
0144-8617/

Rodriguez-Sanchez, Blanco, & López-Quintela, 2000), autoclave (Yang & Pan, 2012), microwave (Khan, El-Toni, et al., 2011) and photochemical reduction (Alarcon et al., 2012; dip Saha, Pal, Kundu, Basu, & Pal, 2010).

Among the methods, chemical reduction was widely studied, due to its advantages of yielding nanoparticles without aggregation, high yield and low preparation cost. The chemical reduction method involves the reduction of silver ion by a reducing agent, such as sodium borohydride (Eom, Ryu, Kim, & Kwon, 2013), hydrazine (Ryu et al., 2005), formamide (Sarkar, Kapoor, & Mukherjee, 2005), formaldehyde (Wu & Hsu, 2008), ascorbic acid (Qin et al., 2010), aniline (Khan, Al-Thabaiti, Obaid, & Al-Youbi, 2011), tyrosine (Khan, AL-Thabaiti, Obaid, Khan, & Al-Youbi, 2012), ethylene glycol (Zhao et al., 2010) and glucose (Shervani & Yamamoto, 2011) in an appropriate medium and in the presence of a suitable stabilizer, such as cetyltrimethylammonium bromide (Khan et al., 2012), sodium citrate (Pinto et al., 2010), polyvinyl pyrrolidone (PVP) (Wang, Qiao, Chen, & Ding, 2005), and polyvinyl alcohol (PVA) (Khanna et al., 2005), which is necessary in protecting the growth of silver particles through aggregation. The particle size and aggregation state of silver nanoparticles are affected by various parameters such as silver ion concentration, reducing agent, molar ratios of silver ion and reducing agent, and stabilizer concentration (Guzman, Dille, & Godet, 2012).

Green synthesis of nanoparticles (Sharma, Yngard, & Lin, 2009) is the field of nanoparticle synthesis and assembly by utilization of biological systems such as fungi (Bhainsa & D'Souza, 2006), bacteria (Fayaza, Girilal, Rahman, Venkatesan, & Kalaichelvan, 2011), plant extracts (Park, Hong, Weyers, Kim, & Linhardt, 2011) and natural occurring polysaccharides, such as chitosan (Wei & Qian, 2008; Wei, Sun, Qian, Ye, & Ma, 2009), starch (Vigneshwaran, Nachane, Balasubramanya, & Varadarajan, 2006), dextran (Bankura et al., 2012), heparin (Huang & Yang, 2004), alginate (Arockianathana, Sekara, Sankara, Kumaran, & Sastry, 2012), cellulose (Peng, Yang, & Xiong, 2013), and hyaluronan (Xia, Cai, Jiang, & Yao, 2011) as stabilizing and/or reducing agents. The development of silver nanoparticles using green synthesis technique has revolutionized the whole field of nanoparticles synthesis. This technique is popular these days because of its vast reserves of plants that are easily accessible, widely distributed, safe to handle, and minimizes the waste and energy costs. The green synthesis of Ag NPs includes selection of solvent medium, reducing agent and non-toxic stabilizing agent, also termed as capping agent, prevents aggregation of the nanoparticles. As these nanoparticles result in significantly low toxicity on adoption of this technique, it can be used for encapsulation of drug or protein molecules. Further research in the field of nanomedicine with respect to Ag NPs is going on worldwide.

Chondroitin sulfates (ChS) are naturally occurring glycosaminoglycans (GAGs) present in the extracellular matrix (ECM) of cartilage that confers to the cartilage desired mechanical properties. ChS is an anionic polyelectrolyte consisting of repeating disaccharide units of β-1,4-linked D-glucuronic acid and β-1,3-linked N-acetyl galactosamine (GalNAc). In biomedical applications, ChS is one type of "neutraceuticals" that are used in the treatment of the symptoms of osteoarthritis and have shown anti-inflammatory activity (Iouv, Dumais, & Du Souich, 2008). ChS is also a component of the dermal layer of the FDA-approved skin substitute (Phillips, 1998) for enhancing wound re-epithelialization without scarring (Kirker, Luo, Nielson, Shelby, & Prestwich, 2002). Moreover, ChS is similar to the endogenous substance, which can be degraded by colonic micro flora; thus, it has been investigated as a matrix material for colon-specific drug delivery (Sintov, Di-Capua, & Rubinstein, 1995; Wang, Wang, & Chiang, 2002). Recently, we have developed a new nano-carrier system made of ChS and chitosan (CS) via an ionic gelation method (Yeh, Cheng, Hu, Huang, & Young, 2011). These hydrophilic nanoparticles showed a high formation yield and a high encapsulation efficiency of protein. Furthermore, in vitro studies showed that ChS–CS NPs were low cytotoxicity and were endocytosed by Caco-2 and HEK-293 cells.

In order to synthesize silver nanoparticles by the chemical reduction method, a reducing agent needs to be added. In addition, reagents such as long-chain thios, long-chain amines, carboxylic compounds, PVP, and PVA are usually needed to be the protecting agents. Here, we present a facile and green method for the synthesis of silver nanoparticles using biocompatible naturally occurring ChS as both reducing and stabilizing agent to prepare negatively charged ChS-capped Ag NPs at room temperature. Because, nanoparticles have a positive zeta potential, can interact with cell membranes expressing negative zeta potential by nonspecific electrostatic interaction, accelerate the cell endocytosis process. Thus, for the purpose of developing a new nano-carrier system with positive surface charge to deliver drug or protein into cells, the ChS-capped Ag NPs was coated with N-[(2-hydroxy-3-trimethylammonium)propyl] chitosan chloride (HTCC) via an ionic gelation method, and the surface charge of Ag NPs was switched from negative to positive.

2. Materials and methods

2.1. Materials

Chondroitin 4-sulfate sodium salt (ChS) from bovine trachea was purchased from Fluka (Buchs, Switzerland). Chitosan (viscosity: 7.5 cps (5 g/l), degree of deacetylation (DD): 90.2%) was purchased from Wako Pure Chemical Industries Ltd. (Osaka, Japan). Silver nitrate was purchased from Merck (Darmstadt, Germany). All aqueous solutions were made using ultrapure water obtained with Milli-Q equipment (Millipore, Billerica, MA, USA).

2.2. Synthesis of ChS-capped Ag NPs

The ChS–Ag NPs were synthesized by the reduction of Ag^+ ions in aqueous medium using ChS as both reducing and stabilizing agent. In a typical preparation process, an aqueous solution of silver nitrate was added dropwise into an aqueous solution of ChS at room temperature while stirring. The mixture was stirred continuously for 5 days. At the pre-determinate intervals (3, 6, 24, 48, 120 h), portions of reaction mixture were taken to measure the surface plasmon resonance (SPR), size and zeta potential immediately. Table 1 summarizes the synthesis conditions used to prepare the ChS–Ag NPs and indicates the ChS/Ag^+ weight ratio of those solutions. For the sake of simplicity the weight ratio will hereafter be referred as the ChS/Ag^+ weight ratio. After reaction, the resulting dispersions were placed under ambient conditions for several weeks. It was observed that the aqueous solution of silver nanoparticles was stable more than 2 months in the as-prepared solution at room temperature. The dependence of particle size and zeta potential on the concentration, weight ratio, reaction time and reaction temperature has been also studied in detail.

The excess unreacted ChS and silver ion remained in suspension were separated from ChS–Ag NPs using Amicon® Ultra-15 centrifugal filter device (100 K) at 5000 × *g* for 10 min, and repeated this procedure three times by adding milli-Q water. The purified ChS–Ag NPs were re-suspended in milli-Q water for TEM image and surface-modification, or they were then lyophilized for FT-IR measurement.

2.3. Synthesis of N-[(2-hydroxy-3-trimethylammonium)propyl] chitosan chloride (HTCC)

HTCC was prepared by a modified method of previous report (Nam, Kim, & Ko, 1999). 12 g of chitosan powder was suspended in

Table 1
Synthesis of ChS–Ag NPs at different concentration, weight ratio and temperature.

Experiment	Final concentration		Weight ratio		Temperature (°C)
	$AgNO_3$ (mM)	ChS (mg/ml)	$ChS/AgNO_3$	ChS/Ag^+	
1	6.25	20	18.8	29.6	25
2	6.25	10	9.4	14.8	25
3	6.25	5	4.7	7.4	25
4	6.25	2.5	2.4	3.7	25
5	1	12.8	75.4	118.6	25
6	1	6.4	37.6	59.3	25
7	1	3.2	18.8	29.6	25
8	1	1.6	9.4	14.8	25
9	1	0.8	4.7	7.4	25
10	6.25	20	18.8	29.6	80
11	1	6.4	37.6	59.3	80

120 mL of milli-Q water. The mixture was stirred for 30 min prior to dropwise addition of 48 g glycidyltrimethylammonium chloride (GTMAC) with continuous stirring. The reaction mixture was stirred at 85 °C overnight. After being precipitated and washed by acetone and methanol, the product was collected by centrifugation. The collected polymer was dissolved in water and dialyzed (Slide-A-Lyzer® Dialysis Cassette G2, 2000 MWCO, 70 ml capacity) against water for 3 days and lyophilized.

2.4. Surface-modification of ChS–Ag NPs with HTCC

HTCC coated ChS–Ag NPs were prepared based on the ionotropic gelation of the cations of HTCC with the anions of ChS–Ag NPs. Preliminary experiments were done in order to determine the aggregation point of NP formation. For this purpose, HTCC was dissolved in Milli-Q water at the concentration of 4 mg/ml. The ChS–Ag NPs suspension solution was added dropwise to a 2 ml of HTCC solutions at room temperature. As soon as the ChS–Ag NPs suspension solution was added to the HTCC solution, the HTCC coated ChS–Ag NPs suspension was formed under magnetic stirring. The ChS–Ag NPs suspension was continuously added until an aggregate was formed in the solution. The volume of ChS–Ag NPs suspension used at the point of aggregation was then recorded, and used as reference volume to calculate the aggregation level by the following equation:

$$\text{Aggregation level } (\%) = \frac{V}{V_a} \times 100$$

where V is the volume of ChS–Ag NPs suspension applied and V_a is the volume of ChS–Ag NPs suspension applied at the aggregation point.

HTCC coated ChS–Ag NPs were formed spontaneously upon incorporation of different volume of ChS–Ag NPs suspension solution to a HTCC aqueous solution under magnetic stirring at room temperature. The agitation was maintained for 5 min in order to allow the stabilization of the system. At the pre-determinate applied volume, the reaction mixtures were taken to measure the particle size and zeta potential immediately.

2.5. Physicochemical characterization of ChS–Ag NPs

Ultraviolet–visible (UV–vis) absorption spectra were recorded on a Perkin Elmer Lambda 35 spectrophotometer (PerkinElmer, Waltham, MA, USA), scanning from 300 to 700 nm. Samples were run in disposable 1.5 mL plastic cuvettes. Milli-Q water was used in the reference cell. Concentrated samples (Ag^+ final concentration = 6.25 mM) were diluted fivefold with Milli-Q water before detection. The measurements were carried out immediately after the pre-determined time along the duration of this study.

The particle size was characterized by photon correlation spectroscopy (Zetasizer Nano-ZS; Malvern Instruments, UK). The instrument contains a 4 mW He–Ne laser operating at a wavelength of 633 nm and an avalanche photodiode (APD) detector. The scattered light was detected at an angel of 173°. Raw data were subsequently correlated to the mean hydrodynamic size by cumulants analysis (Z-average mean). The zeta potentials (ζ) of all ChS–Ag NPs were analyzed using laser Doppler anemometry (Zetasizer Nano-ZS; Malvern Instruments, UK). The measurements were carried out immediately at the pre-determined time intervals and all measurements were done at 25 °C.

Their Fourier transform-infrared (FT-IR) spectra were taken with KBr pellets on a PerkinElmer Spectrum One FTIR (PerkinElmer, Waltham, MA, USA).

The morphology of ChS–Ag NPs after purified as previous procedure were examined on a Jeol JEM-1200 EXII transmission electron microscopy (TEM; Jeol, Tokyo, Japan). A typical method for preparing TEM samples was as follows: one drop of ChS–Ag NP suspension was deposited on a 200-mesh Formvar/carbon-coated copper grid, and excess solution was removed by wicking with filter paper to avoid particle aggregation. The images were examined using a TEM at 80 kV.

3. Results and discussion

3.1. Green synthesis of ChS-capped Ag NPs

Chondroitin sulfate (ChS) was used as the capping agents because of its good biocompatibility and biodegradability. ChS is an anionic polyelectrolyte containing negatively charged sulfate and carboxylate groups. Recently, ChS has been used as stabilizing agent of gold nanoparticles which were prepared from $HAuCl_4$ aqueous solution using sodium borohydride as a reducing agent (Li et al., 2011), but no report has appeared describing the use of this glycosaminoglycan as a reducing or stabilizing agent in the synthesis of silver nanoparticles. The procedure for the synthesis of Ag NPs using ChS as both reducing and stabilizing agent is quite simple. In a typical preparation, the aqueous solution of $AgNO_3$ was mixed with the aqueous solution of ChS and stirred at the room temperature without purged with nitrogen or argon to remove oxygen, and any assisted by microwave, autoclave, laser ablation, γ-ray irradiation or UV irradiation. In the present approach, water is utilized as the environmentally benign solvent throughout the preparation.

3.2. Studies of ChS–Ag NP formation using UV–vis spectroscopy

The gradual evolution of silver nanoparticles was monitored using UV–vis spectroscopy. Fig. 1a and b shows the UV–vis absorption spectra of the silver nanoparticles at different reaction time intervals. The characteristic surface plasmon resonance (SPR) peak

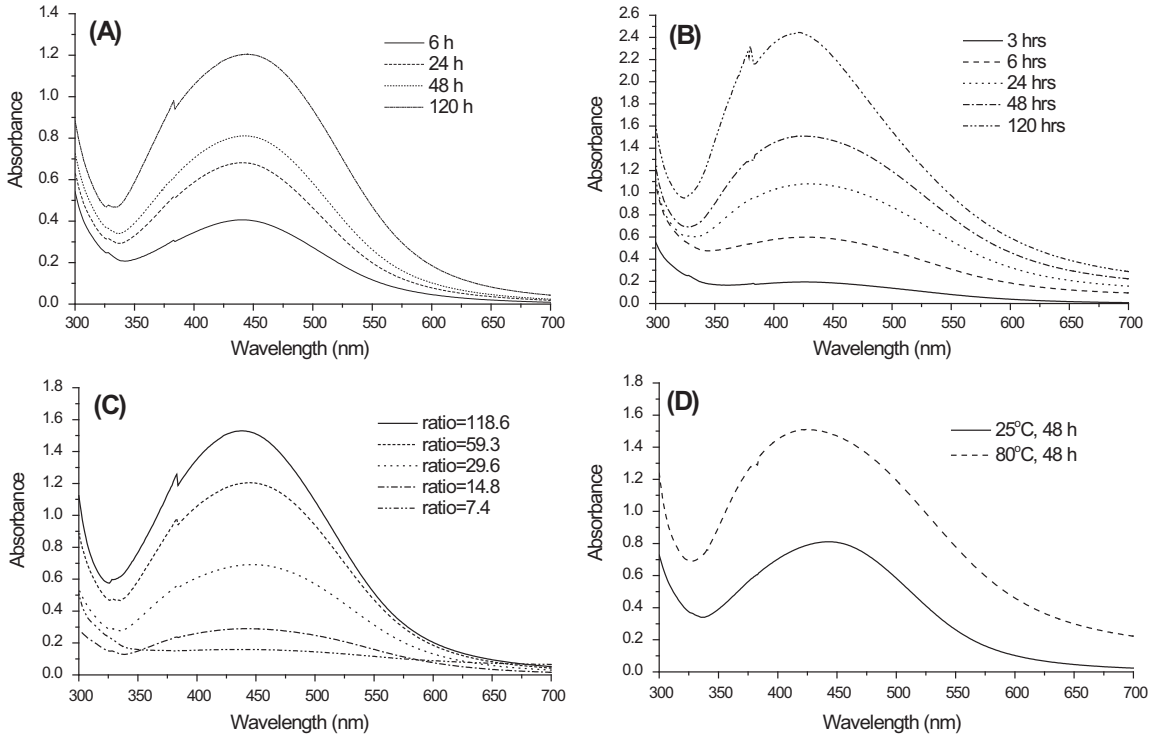

Fig. 1. UV–vis spectra of as-prepared ChS-capped Ag NPs solutions: (A) effects of the reaction time at room temperature (experiment 6); (B) effects of the reaction time at 80 °C (experiment 11); (C) effects of weight ratio of ChS/Ag^+ at room temperature (experiment 5–9); and (D) effects of the temperature at the same reaction time (experiment 6 and 11).

at around 443 nm obtained at different reaction times confirmed the formation of silver nanoparticles. Gradually longer reaction time, from 3 to 120 h, increased the corresponding peak intensities with concomitant blue shift, but no obviously peaks broaden occurred. The increase in intensities indicated the increase in the concentration of the silver nanoparticles. The small blue shift of the SPR peaks indicates a little decrease in the particle size as the reaction progress.

In order to study the effect of ChS concentration on silver nanoparticles preparation, the reactions were carried out at different weight ratios of ChS/Ag^+. Silver colloidal obtained at lowest weight ratios appeared light red. As the weight ratios increased, the color of the solution gradually changed to red brown and the SPR peak increased in its intensity (Fig. 1c). These results indicated that the higher weight ratios, the higher yields of silver nanoparticles were produced at the same reaction time.

For studying the influence of reaction temperature, the reactions were carried out at 25 and 80 °C under the same reactant composition. The effects of the temperature on silver nanoparticles formation are shown in Fig. 1d, showing a blue shift of the SPR peak with increase in the intensity and broadness at high temperature. The results suggested that silver nanoparticles with higher yields and wider size distribution could be obtained at a higher reaction temperature.

3.3. Measurement of particle size by dynamic light scattering (Filella, Zhang, Newman, & Buffle, 1997; Jans, Liu, Austin, Maes, & Huo, 2009; Murdock, Braydich-Stolle, Schrand, Schlager, & Hussain, 2008)

Table 2 shows the *Z*-average diameter and polydispersity index valve (PDI) obtained from dynamic light scattering (DLS) corresponds to the experiments in Table 1. DLS is a non-invasive technique for measuring the size of nanoparticles in a dispersion. The technique measures the time-dependent fluctuations in the intensity of scattered light from a suspension of particles undergoing random, Brownian motion. Analysis of these intensity fluctuations allows for the determination of the diffusion coefficients, which in turn yield the particle size through the Stokes–Einstein equation. Thus, the *Z*-average is the mean hydrodynamic diameter and the PDI is an estimate of the width of the distribution.

The influence of the concentration, weight ratio, temperature and the reaction time on the *Z*-average of ChS–Ag NPs is shown in Table 2. NPs were obtained by using final concentration of 1 and 6.25 mg/ml Ag^+ solutions at the weight ratio range from 3.7 to 118.6. Obviously, the *Z*-average increased with the increase in weight ratio at a fixed Ag^+ concentration. Table 2 also shows the tendency toward a higher *Z*-average with a higher Ag^+ concentration at a fixed weight ratio. On the contrast, the *Z*-average and PDI only has a little change as the reactions proceed at the room temperature. When the reaction performed at 80 °C, the *Z*-average and PDI values became bigger as the reaction time increased. The *Z*-average and PDI values are sensitive to the presence of aggregates, this phenomenon represents some aggregates occurred at the longer reaction time.

Fig. 2a–d shows the intensity size distribution obtained for the experiments 1-4 measured at the different reaction time intervals. The plot shows the relative percentage of light scattered by particles (on the *Y*-axis) in various size classes (on the *X*-axis). The intensity size distribution obtained implies that there are no significant aggregates present in these samples at the room temperature. But it appeared that a consider amount of smaller size particles were formed as the reaction proceed.

Normally, the intensity particle size distribution shows a broaden peaks cover a wide range of size, this is due to DLS is a low resolution technique being able to resolve materials with a factor of 3 difference in their sizes, which means if the sample was to be measured by DLS, it would not be possible to resolve different sized peaks for the various particle species, i.e. single particles,

Table 2
Z-average diameter (*d*. nm) and polydispersity index valve obtained by DLS, and zeta potential (ζ) obtained from laser Doppler anemometry at different time intervals.

Exp.[a]	3 h		6 h		24 h		48 h		120 h	
	***Z*-Average** PDI	ζ (mV)	***Z*-Average** PDI	ζ (mV)	***Z*-Average** PDI	ζ (mV)	***Z*-Average** PDI	ζ (mV)	***Z*-Average** PDI	ζ (mV)
1	–	–	**87.73** 0.140	−49.5	**89.61** 0.127	−46.5	**87.28** 0.113	−43.9	**85.55** 0.124	−51.9
2	–	–	**76.72** 0.202	−35.4	**68.65** 0.186	−42.3	**68.97** 0.151	−41.8	**69.40** 0.180	−50.0
3	–	–	**50.93** 0.228	−30.0	**46.59** 0.170	−36.2	**45.85** 0.258	−41.8	**44.52** 0.340	−47.6
4	–	–	**40.23** 0.264	−23.3	**38.96** 0.291	−41.6	**31.91** 0.472	−38.8	**33.10** 0.513	−45.7
5	–	–	**98.36** 0.093	−40.0	**103.2** 0.112	−45.3	**104.0** 0.122	−43.7	**102.2** 0.106	−46.5
6	–	–	**76.73** 0.136	−34.0	**79.87** 0.130	−46.2	**79.35** 0.109	−48.7	**77.60** 0.115	−50.0
7	–	–	**58.42** 0.162	−46.6	**64.51** 0.217	−52.4	**64.50** 0.237	−46.5	**71.09** 0.280	−54.1
8	–	–	**53.58** 0.121	−37.8	**54.14** 0.120	−44.3	**54.94** 0.142	−47.0	**58.27** 0.146	−46.4
9	–	–	**55.03** 0.116	−32.8	**56.46** 0.118	−41.5	**56.49** 0.117	−39.5	**58.57** 0.145	−43.0
10	**97.0** 0.131	−50.7	**86.58** 0.120	−48.7	**76.21** 0.257	−52.5	**101.9** 0.444	−54.2	**89.50** 0.381	−57.8
11	**132.8** 0.167	−48.7	**167.2** 0.237	−49.6	**151.6** 0.414	−54.6	**144.9** 0.508	−56.0	**148.2** 0.710	−57.3

[a] The experiments correspond to the experiments in Table 1.

aggregates of two particles, aggregates of three particles, etc. So a mixture of single particles and aggregates made of two, three or four particles would be expected to give a broad single peak with the result obtained being influenced by the larger particles present as they would scatter the majority of the light.

Fig. 2e–h shows the effect of the reaction temperature on the intensity size distribution measured at the different time intervals. Obviously, aggregates were formed at 80 °C when the reaction time longer than 24 h. The results were consistent with the conclusions obtained from the *Z*-average, PDI values and UV–vis.

3.4. Zeta potential (ζ)

The stability of colloidal dispersions is determined by the sum of attractive forces (Van der Waal) and the repulsive forces (electrostatic) which particles experience as they approach one another. To maintain dispersion stability, the repulsive forces must be dominant. The zeta potential is the electrical potential at the slipping plane (hydrodynamic plane of shear). For electrostatically stabilized dispersions, the higher the value of zeta potential, the more stable the dispersion is likely to be, and the stability dividing line is generally considered to be ±30 mV. The absolute valve of zeta potential in Table 2 are almost all larger than 30 mV, represented the ChS–Ag NPs formed by this method showed a high stability in the reaction medium. Table 2 also shows the tendency toward an increasing the weight ratio with an increase in the absolute valve of zeta potential, indicated that more negatively charged ChS capped in the surface of Ag NP at the higher weight ratio, thus increased the particle size of ChS-capped Ag NPs. These results can explain the phenomenon that the *Z*-average increased with the increase weight ratio observed by DLS.

3.5. Stability of ChS–Ag NPs

So far, UV–vis absorption has been used as a common tool to monitor metal nanoparticle aggregation, because the aggregation causes a shift or broadening of the SPR of the metal nanoparticle. However, such measurements are often low sensitivity. The aggregation can be detected by UV–vis spectroscopy only when the aggregation level is significant enough to cause a color change. As a particle size measurement tool, DLS could be a more sensitive tool for nanoparticle aggregation study than UV–vis spectroscopy (Zimbone, Calcagno, Messina, Baeri, & Compagnini, 2011). We examined the aggregation behavior of ChS–Ag NPs stocked in reaction medium and in water at different time intervals using DLS. The ChS–Ag NPs stocked in reaction medium and in water are highly stable as there is no precipitate and color change visually observed. Fig. 3 shows the intensity size distribution obtained for ChS–Ag NPs measured at different time intervals. When the as-prepared ChS–Ag NPs stocked in reaction medium at the room temperature, no aggregation peak and peak broaden was observed by day 56 (Fig. 3a). However, the peak became broaden, when the purified ChS–Ag NPs stocked in water by day 21 (Fig. 3b). The mixture of more aggregates made of two, three or four particles would be expected to give a broad single peak. The results indicated the ChS–Ag NPs stocked in reaction medium is more stable than stocked in water.

3.6. FT-IR

Fig. 4 shows the FT-IR spectra of pure ChS and ChS–Ag NPs. The characterization peaks in the pure ChS spectrum are 3412 cm^{-1} (—OH and —NH_2 stretching), 1626 cm^{-1} (amide I band), 1609 cm^{-1} (asymmetric CO_2^- stretching), 1571 cm^{-1} (N—H deformation), 1257 cm^{-1} (asymmetric SO_2 stretching) and 1122 cm^{-1} (symmetric SO_2 stretching). In ChS–Ag NPs the 1626 cm^{-1} peak of the amide I band shifted to 1645 cm^{-1}, the 1609 cm^{-1} peak of the asymmetric CO_2^- stretching shifted to 1619 cm^{-1}, the 1257 cm^{-1} (asymmetric SO_2 stretching) shifted to 1250 cm^{-1} and the 1122 cm^{-1} (symmetric SO_2 stretching) shifted to 1129 cm^{-1}. These differences indicated that a chemical bond between the silver atom and oxygen atom of sulfate and carboxylate groups in ChS has been formed. By this way, the ChS molecules are strongly adsorbed on the surface of silver nanoparticles, preventing the silver nanoparticles from agglomeration. The FT-IR results confirm once again that the ChS as capping agent or stabilizer plays an important role in the formation and growth of the silver nanoparticles.

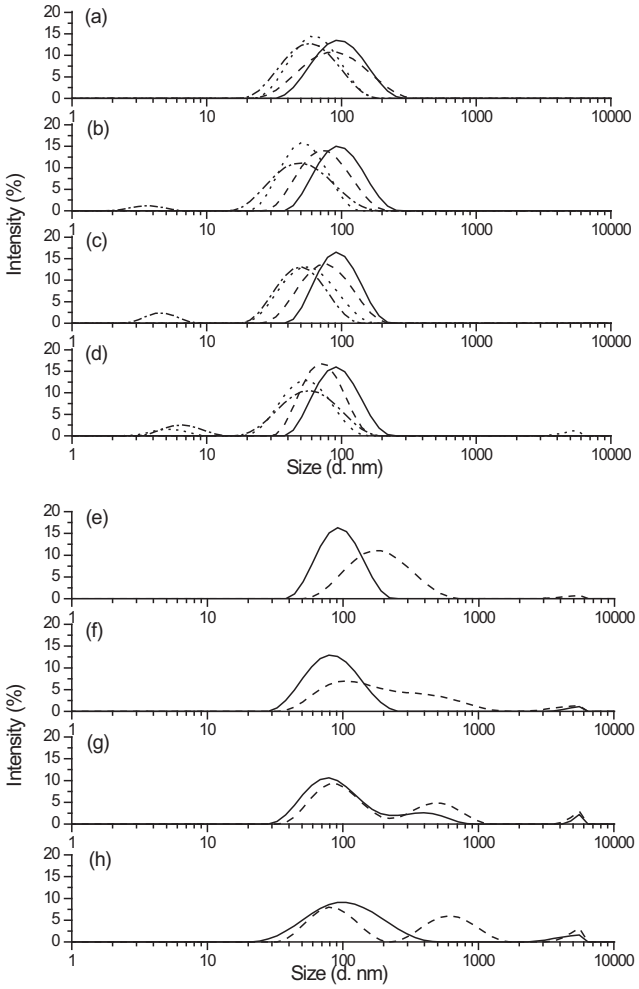

Fig. 2. Intensity size distribution of ChS-capped Ag NPs obtained by DLS at different time intervals: (a) 6 h; (b) 24 h; (c) 48 h; and (d) 120 h. Experiment 1 (solid); Experiment 2 (dash); Experiment 3 (dot); Experiment 4 (dash dot). Intensity size distribution of ChS-capped Ag NPs obtained by DLS at 80 °C and at different reaction times: (e) 6 h; (f) 24 h; (g) 48 h; and (h) 120 h. Experiment 10 (solid); Experiment 11 (dash).

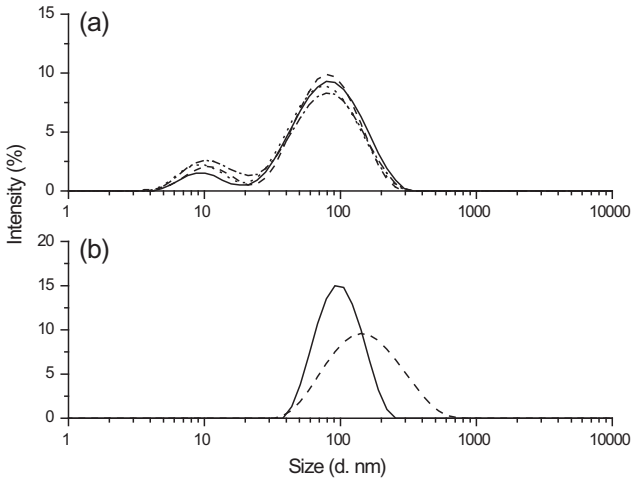

Fig. 3. (a) Intensity size distribution of as-prepared ChS-capped Ag NPs stocked in reaction medium at room temperature on day 3 (solid), day 11 (dash), day 31 (dot) and day 56 (dash dot). (b) Intensity size distribution of purified ChS-capped Ag NPs stocked in milli Q water at room temperature on day 1 (solid) and day 22 (dash).

3.7. TEM image of ChS–Ag NPs

Typical TEM images of purified ChS–Ag NPs are shown in Fig. 5a and b. The figure shows that the resultant particles are very fine and well-dispersion. The nanoparticles obtained are all spherical in shape, approximately <20 nm in diameter. However, the *Z*-average diameter (76.8 nm) obtained from DLS is much higher than the diameter obtained from TEM image. Fig. 5c shows the size distribution of purified ChS-capped Ag NPs obtained by DLS before applied to the TEM image measurement. The size distribution obtained is a trimodal with peak means of 3.6 nm, 11.7 nm and 114.0 nm, respectively. The intensity size distribution (solid line) obtained implies that there are significant aggregates present in this sample. However, conversion into a volume (or mass) based size distribution (dash line) shows that the aggregates are present in low concentration. The result can be further converted into a number based size distribution (dot line). This distribution is monomodal with a

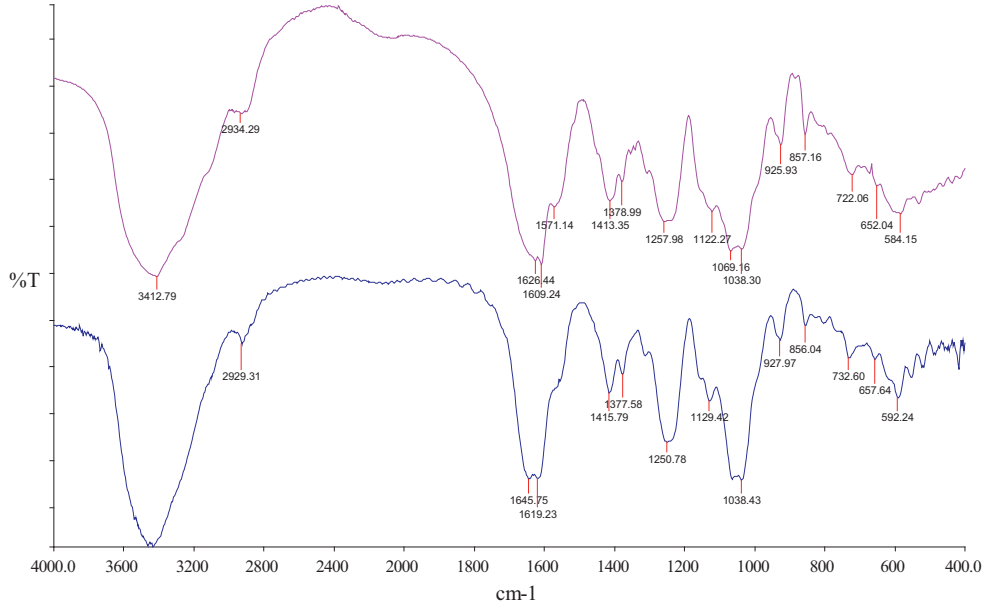

Fig. 4. FT-IR spectra of pure ChS (upper) and purified ChS-capped Ag NPs (lower).

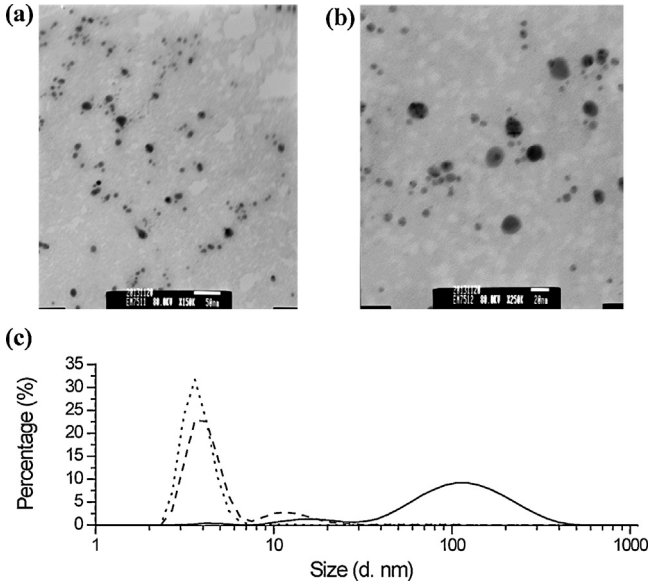

Fig. 5. TEM image of purified ChS-capped Ag NPs: (a) ×150 K, bar = 50 nm; (b) ×250 K, bar = 20 nm; (c) size distribution of purified ChS-capped Ag NPs obtained by DLS before applied to the TEM image measurement. Intensity size distribution (solid); volume size distribution (dash); number size distribution (dot). (The transformation from the intensity data into volume is performed using Mie theory.).

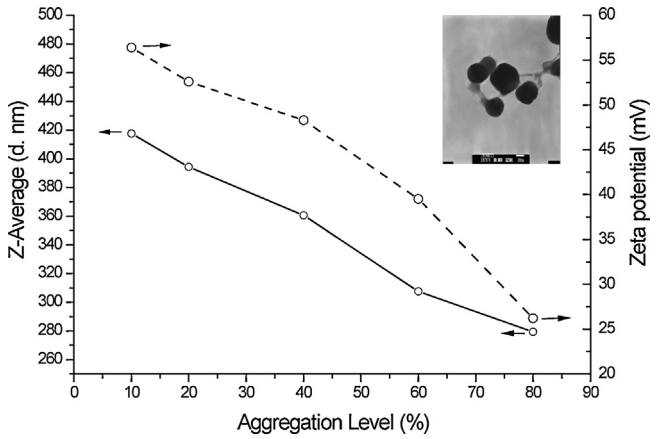

Fig. 6. The influence of aggregation level on the particles size (*Z*-average) and zeta potential of ChS-capped Ag NPs coated with HTCC. Inset: TEM imaging of HTCC coated ChS Ag NPs (250 K×, bar = 50 nm). In this experiment, the particle size and zeta potential of purified ChS Ag NPs using to interact with HTCC is 120 nm and −58 mV, respectively. Initial concentration: HTCC (4 mg/ml).

peak mean at 3.6 nm. The result suggests that if this sample were characterized using a number based technique, such as TEM, the vast majority of particles visible would be small ones. The presence of large particles would only be seen if sufficient numbers were counted. Even though, on a number basis, this sample contains very few aggregates, they scatter a significant amount of light contributing to the major peak in the intensity size distribution. Therefore such a sample would be expected to give quite different results when analyzed by dynamic light scattering and TEM.

3.8. Surface-modification of ChS–Ag NPs

HTCC is a partially quaternized derivative of chitosan, it shows better hydroscopic property, moisture retentiveness, mucoadhesivity and permeability enhancing property comparing with chitosan. It has been shown that HTCC significantly enhanced the absorption across mucosal epithelia even in neutral or basic environment (Thanou, Verhoef, & Junginger, 2001; Wu et al., 2012). In 2010, our laboratory successfully developed a new nano-carrier system made of ChS and chitosan (CS) (Yeh et al., 2011). Our study was based on inducing its gelation by controlling the interaction of CS with the counter ion ChS. In this sense, it is known that the intermolecular linkages created between the negatively charged sulfate and carboxylate groups of ChS and the positively charged amino group of CS are responsible for the success of the gelation process. Thus, we proposed that similar gelation reaction could occur between the sulfate and carboxylate groups of ChS–Ag NPs and trimetylammonium salts of HTCC. As predict, the opalescent suspension was formed when ChS–Ag NPs suspension added to the HTCC aqueous solution in neutral condition. It can be noted that the weight ratio of ChS–Ag NP/HTCC mostly held constant at the aggregation point at a specific pH. This phenomenon is same as the result in the ChS/CS nanoparticles formation.

Fig. 6 depicts the effects of aggregation level on the particle size and zeta potential. Usually, we are accustomed to use aggregation level representing how close we approached to the aggregation point. Obviously, the particle size and zeta potential decreased as the weight ratio close to the aggregation point, and all particle sizes larger than the original size (120 nm), and the zeta potential switched from −58 mV to positive value. This phenomenon represented that the positively charged HTCC can interact with the negatively charged ChS–Ag NPs via ionic gelation to form a new HTCC coated ChS–Ag NP. The inset of Fig. 6 shows the TEM imaging of HTCC coated ChS–Ag NPs, the particle obtained are close to spherical in shape, approximately <100 nm in diameter. Again, the particles size measured by TEM smaller than the *Z*-average (280 nm) measured by DLS method.

4. Conclusion

In this study, a one-step green synthesis of stable ChS–Ag NPs was developed. The synthesis was carried out in a stirring aqueous medium at the room temperature using ChS as both reducing and stabilizing agent. The reaction temperature, reaction time, concentration and the weight ratio of ChS/Ag^+ had obvious effects on the amount of Ag NPs formation and on the particle size distribution. The results indicated that increased the weight ratio of ChS/Ag^+ and the concentration of Ag^+ corresponded to increase average particle size. Raise the reaction temperature can accelerate the formation rate of Ag NPs, but longer reaction time (>24 h) led to the aggregates formed. Meanwhile, the Ag NPs stocked in reaction medium were more stable than those stocked in water. Generally, the as-synthesized ChS–Ag NPs are well-dispersed, spherical in shape with a narrow size distribution and very stable in reaction medium. At the same time, HTCC coated ChS-capped Ag NPs can be easily prepared by simple mixed ChS-capped Ag NPs with HTCC aqueous solution via an ionic gelation method and the surface charge of Ag NPs was changed from negative to positive. The positive surface charge of HTCC coated ChS-capped Ag NPs can interact with negative charged cell membranes by electrostatic interactions, accelerate the cell endocytosis process, and has great potential become a new nano-carrier system to delivery drug or protein into cells.

Acknowledgments

The authors would like to acknowledge the financial support from National Defense Medical Center, Grant No. 102-B18, (2013). Thanks to Ms. Chia-Ying Chien of Precious Instrument Center (National Taiwan University) for the assistance in TEM experiments.

References

Abid, J. P., Wark, A. W., Brevetm, P. F., & Girault, H. H. (2002). Preparation of silver nanoparticles in solution from a silver salt by laser irradiation. *Chemical Communications*, *7*, 792–793.

Alarcon, E. I., Udekwu, K., Skog, M., Pacioni, N. L., Stamplecoskie, K. G., González-Béjar, M., et al. (2012). The biocompatibility and antibacterial properties of collagen-stabilized, photochemically prepared silver nanoparticles. *Biomaterials*, *33*(19), 4947–4956.

Amidi, M., Mastrobattista, E., Jiskoot, W., & Hennink, W. E. (2010). Chitosan-based delivery systems for protein therapeutics and antigens. *Advanced Drug Delivery Reviews*, *62*(1), 59–82.

Arockianathana, P. M., Sekara, S., Sankara, S., Kumaran, B., & Sastry, T. P. (2012). Evaluation of biocomposite films containing alginate and sago starch impregnated with silver nano particles. *Carbohydrate Polymers*, *90*(1), 717–724.

Bankura, K. P., Maity, D., Mollick, M. M. R., Mondal, D., Bhowmick, B., Bain, M. K., et al. (2012). Synthesis, characterization and antimicrobial activity of dextran stabilized silver nanoparticles in aqueous medium. *Carbohydrate Polymers*, *89*(4), 1159–1165.

Bhainsa, K. C., & D'Souza, S. F. (2006). Extracellular biosynthesis of silver nanoparticles using the fungus *Aspergillus fumigatus*. *Colloids and Surfaces B: Biointerfaces*, *47*(2), 160–164.

Chen, P., Song, L. Y., & Liu, Y. K. (2007). Synthesis of silver nanoparticles by γ-ray irradiation in acetic water solution containing chitosan. *Radiation Physics and Chemistry*, *76*(7), 1165–1168.

dip Saha, S., Pal, A., Kundu, S., Basu, S., & Pal, T. (2010). Photochemical green synthesis of calcium-alginate-stabilized Ag and Au nanoparticles and their catalytic application to 4-nitrophenol reduction. *Langmuir*, *26*(4), 2885–2893.

Eom, S. Y., Ryu, S. L., Kim, H. L., & Kwon, C. H. (2013). Systematic preparation of colloidal silver nanoparticles for effective SERS substrates. *Colloids and Surfaces A: Physicochemical and Engineering Aspects*, *422*, 39–43.

Fayaza, A. M., Girilal, M., Rahman, M., Venkatesan, R., & Kalaichelvan, P. T. (2011). Biosynthesis of silver and gold nanoparticles using thermophilic bacterium *Geobacillus stearothermophilus*. *Process Biochemistry*, *46*(10), 1958–1962.

Filella, M., Zhang, J., Newman, M., & Buffle, J. (1997). Analytical application of photo correlation spectroscopy for size distribution measurements of natural colloidal suspensions: Capabilities and limitations. *Colloids and Surfaces A: Physicochemical and Engineering Aspects*, *120*(1–3), 27–46.

Guzman, M., Dille, J., & Godet, S. (2012). Synthesis and antibacterial activity of silver nanoparticles against gram-positive and gram-negative bacteria. *Nanomedicine: Nanotechnology, Biology and Medicine*, *8*(1), 37–45.

Huang, H., & Yang, X. (2004). Synthesis of polysaccharide-stabilized gold and silver nanoparticles: A green method. *Carbohydrate Research*, *339*(15), 2627–2631.

Iouv, M., Dumais, G., & Du Souich, P. (2008). Anti-inflammatory activity of chondroitin sulfate. *Osteoarthritis and Cartilage*, *16*, S14–S18.

Jans, H., Liu, X., Austin, L., Maes, G., & Huo, Q. (2009). Dynamic light scattering as a powerful tool for gold nanoparticle bioconjugation and biomolecular binding studies. *Analytical Chemistry*, *81*(22), 9425–9432.

Khan, A., El-Toni, A. M., Alrokayan, S., Alsalhi, M., Alhoshan, M., & Aldwayyan, A. S. (2011). Microwave-assisted synthesis of silver nanoparticles using poly-N-isopropylacrylamide/acrylic acid microgel particles. *Colloids and Surfaces A: Physicochemical and Engineering Aspects*, *377*(1–3), 356–360.

Khan, Z., Al-Thabaiti, S. A., Obaid, A. Y., & Al-Youbi, A. O. (2011). Preparation and characterization of silver nanoparticles by chemical reduction method. *Colloids and Surfaces B: Biointerfaces*, *82*(2), 513–517.

Khan, Z., A.L-Thabaiti, S. A., Obaid, A. Y., Khan, Z. A., & Al-Youbi, A. A. O. (2012). Shape-directing role of cetyltrimethylammonium bromide in the preparation of silver nanoparticles. *Journal of Colloid and Interface Science*, *367*(1), 101–108.

Khanna, P. K., Singh, N., Charan, S., Subbarao, V. V. V. S., Gokhale, R., & Mulik, U. P. (2005). Synthesis and characterization of Ag/PVA nanocomposite by chemical reduction method. *Materials Chemistry and Physics*, *93*(1), 117–121.

Kirker, K. R., Luo, Y., Nielson, J. H., Shelby, J., & Prestwich, G. D. (2002). Glycosaminoglycan hydrogel films as bio-interactive dressings for wound healing. *Biomaterials*, *23*(17), 3661–3671.

Li, W., Li, X., Su, H., Zhao, S., Li, Y., & Hu, J. (2011). Facile synthesis of chondroitin sulfate-stabilized gold nanoparticles. *Materials Chemistry and Physics*, *125*(3), 518–521.

Murdock, R. C., Braydich-Stolle, L., Schrand, A. M., Schlager, J. J., & Hussain, S. M. (2008). Characterization of nanomaterial dispersion in solution prior to in vitro exposure using dynamic light scattering technique. *Toxicological Sciences*, *101*(2), 239–253.

Nam, C. W., Kim, Y. H., & Ko, S. W. (1999). Modification of polyacrylonitrile (PAN) fiber by blending with N-(2-Hydroxy)propyl-3-trimethylammonium chitosan chloride. *Journal of Applied Polymer Science*, *74*(9), 2258–2265.

Park, Y., Hong, Y. N., Weyers, A., Kim, Y. S., & Linhardt, R. J. (2011). Polysaccharides and phytochemicals: A natural reservoir for the green synthesis of gold and silver nanoparticles. *IET Nanobiotechnology*, *5*(3), 69–78.

Peng, H., Yang, A., & Xiong, J. (2013). Green, microwave-assisted synthesis of silver nanoparticles using bamboo hemicelluloses and glucose in an aqueous medium. *Carbohydrate Polymers*, *91*(1), 348–355.

Phillips, T. J. (1998). New skin for old. Developments in biological skin substitutes. *Archives of Dermatology*, *134*(3), 344–349.

Pinto, V. V., Ferreira, M. J., Silva, R., Santos, H. A., Silva, F., & Pereira, C. M. (2010). Long time effect on the stability of silver nanoparticles in aqueous medium: Effect of the synthesis and storage conditions. *Colloids and Surfaces A: Physicochemical and Engineering Aspects*, *364*(1–3), 19–25.

Qin, Y., Ji, X., Jing, J., Liu, H., Wu, H., & Yang, W. (2010). Size control over spherical silver nanoparticles by ascorbic acid reduction. *Colloids and Surfaces A: Physicochemical and Engineering Aspects*, *372*(1–3), 172–176.

Reicha, F. M., Sarhan, A., Abdel-Hamid, M. I., & El-Sherbiny, I. M. (2012). Preparation of silver nanoparticles in the presence of chitosan by electrochemical method. *Carbohydrate Polymers*, *89*(1), 236–244.

Rodriguez-Sanchez, L., Blanco, M. C., & López-Quintela, M. A. (2000). Electrochemical synthesis of silver nanoparticles. *Journal of Physical Chemistry B*, *104*(41), 9683–9688.

Ryu, B. H., Choi, Y., Park, H. S., Byun, J. H., Kong, K., Lee, J. O., et al. (2005). Synthesis of highly concentrated silver nanosol and its application to inkjet printing. *Colloids and Surfaces A: Physicochemical and Engineering Aspects*, *270–271*, 345–351.

Sarkar, A., Kapoor, S., & Mukherjee, T. (2005). Synthesis of silver nanoprisms in formamide. *Journal of Colloid and Interface Science*, *287*(2), 496–500.

Sharma, V. K., Yngard, R. A., & Lin, Y. (2009). Silver nanoparticles: Green synthesis and their antimicrobial activities. *Advances in Colloid and Interface Science*, *145*(1–2), 83–96.

Shervani, Z., & Yamamoto, Y. (2011). Carbohydrate-directed synthesis of silver and gold nanoparticles: Effect of the structure of carbohydrates and reducing agents on the size and morphology of the composites. *Carbohydrate Research*, *346*(5), 651–658.

Sintov, A., Di-Capua, N., & Rubinstein, A. (1995). Cross-linked chondroitin sulphate: Characterization for drug delivery purposes. *Biomaterials*, *16*(6), 473–478.

Thanou, M., Verhoef, J. C., & Junginger, H. E. (2001). Oral drug absorption enhancement by chitosan and its derivatives. *Advanced Drug Delivery Reviews*, *52*(2), 117–126.

Vigneshwaran, N., Nachane, R. P., Balasubramanya, R. H., & Varadarajan, P. V. (2006). A novel one-pot 'green' synthesis of stable silver nanoparticles using soluble starch. *Carbohydrate Research*, *341*(12), 2012–2018.

Wang, H., Qiao, X., Chen, J., & Ding, S. (2005). Preparation of silver nanoparticles by chemical reduction method. *Colloids and Surfaces A: Physicochemical and Engineering Aspects*, *256*(2–3), 111–115.

Wang, L. F., Wang, J. M., & Chiang, Y. L. (2002). Insolubilization of sodium chondroitin sulfate by forming a semi-interpenetrating polymer network with acrylic acid: A potential carrier for colon-specific drug delivery. *Journal of Applied Polymer Science*, *85*(1), 114–122.

Wei, D., & Qian, W. (2008). Facile synthesis of Ag and Au nanoparticles utilizing chitosan as a mediator agent. *Colloids and Surfaces B: Biointerfaces*, *62*(1), 136–142.

Wei, D., Sun, W., Qian, W., Ye, Y., & Ma, X. (2009). The synthesis of chitosan-based silver nanoparticles and their antibacterial activity. *Carbohydrate Research*, *344*(17), 2375–2382.

Wu, R. T., & Hsu, S. L. C. (2008). Preparation of highly concentrated and stable suspensions of silver nanoparticles by an organic base catalyzed reduction reaction. *Materials Research Bulletin*, *43*(5), 1276–1281.

Wu, Y., Wei, W., Zhou, M., Wang, Y., Wu, J., Ma, G., et al. (2012). Thermal-sensitive hydrogel as adjuvant-free vaccine delivery system for H5N1intranasal immunization. *Biomaterials*, *33*(7), 2351–2360.

Xia, N., Cai, Y., Jiang, T., & Yao, J. (2011). Green synthesis of silver nanoparticles by chemical reduction with hyaluronan. *Carbohydrate Polymers*, *86*(2), 956–961.

Yang, J., & Pan, J. (2012). Hydrothermal synthesis of silver nanoparticles by sodium alginate and their applications in surface-enhanced Raman scattering and catalysis. *Acta Materialia*, *60*(12), 4753–4758.

Yeh, M. K., Cheng, K. M., Hu, C. S., Huang, Y. C., & Young, J. J. (2011). Novel protein-loaded chondroitin sulfate-chitosan nanoparticles: Preparation and characterization. *Acta Biomaterialia*, *7*(10), 3804–3812.

Zhang, W. Z., Qiao, X. L., & Chen, J. G. (2006). Synthesis and characterization of silver nanoparticles in AOT microemulsion system. *Chemical Physics*, *300*(3), 495–500.

Zhao, T., Suna, R., Yu, S., Zhang, Z., Zhou, L., Huang, H., et al. (2010). Size-controlled preparation of silver nanoparticles by a modified polyol method. *Colloids and Surfaces A: Physicochemical and Engineering Aspects*, *366*(1–3), 197–202.

Zimbone, M., Calcagno, L., Messina, G., Baeri, P., & Compagnini, G. (2011). Dynamic light scattering and UV–vis spectroscopy of gold nanoparticles solution. *Materials Letters*, *65*(19–20), 2906–2909.